Available online at www.sciencedirect.com
ScienceDirect
Journal of Nuclear Materials 356 (2006) 308–320
journal of nuclear materials
www.elsevier.com/locate/jnucmat

Assessment of the lifetime of the beam window of MEGAPIE target liquid metal container

Y. Dai [a,*], J. Henry [b], T. Auger [c], J.-B. Vogt [d], A. Almazouzi [e], H. Glasbrenner [a], F. Groeschel [a]

[a] *Paul Scherrer Institut, 5232 Villigen PSI, Switzerland*
[b] *Commissariat a l'Energie Atomique, CEA Saclay, 91191 Gif-sur-Yvette cedex, France*
[c] *CNRS, CECM, 94407 Vitry sur Seine, France*
[d] *Université de Lillel, UMR CNRS 8517, 59655 Villeneuve d'Ascq cedex, France*
[e] *SCK/CEN, Boeretang 200, 2400 Mol, Belgium*

Abstract

The lifetime of the beam window of the T91 liquid Pb–Bi container in the MEGAPIE target is discussed based on the present knowledge of lead bismuth eutectic (LBE) corrosion, embrittlement and radiation effects in relevant conditions. In the MEGAPIE target, since the high hydrogen production will likely reduce the oxygen content to a low level, LBE corrosion may reduce the wall thickness up to 2%. In addition, the corrosion induced grain boundary dissolution will promote LBE embrittlement on the T91 steel in the beam window. The DBTT data and fracture toughness values of T91 specimens tested in contact with LBE suggest a lower bound of the lifetime of the T91 beam window to be limited to a dose of 6 dpa, corresponding to 2.4 Ah proton charge to be received by the target in about 20 weeks in the normal operation condition.

1. Introduction

In the MEGAPIE (Megawatt pilot target experiment) target to be operated in the Swiss spallation neutron source (SINQ) [1], the main structural materials are austenitic steel 316L (SS 316L), martensitic steel T91 and aluminum alloy $AlMg_3$. SS 316L is used for all the components inside the lower liquid metal container (LLMC) such as the main flow guide tube, the by-pass flow tube, the fill and drawn tube and the central rod. The T91 steel is selected for the most critical component, the LLMC. The $AlMg_3$ alloy is used for the lower target enclosure (LTE), the safety-container as in a normal solid target operated in SINQ. The behaviors of these structural materials under irradiation are essential for the safe operation of the MEGAPIE target [2].

In the scientific R&D support program, Task X7 is assigned for studying solid–liquid interface related issues, and Task X10 is for investigating the radiation effects on structural materials. In Tasks X7 and X10 activities, the main efforts have been concentrated on the T91 steel because the LLMC will be subjected to intensive proton and neutron irradi-

* Corresponding author. Tel.: +41 56 310 4171; fax: +41 56 310 4529.
E-mail address: yong.dai@psi.ch (Y. Dai).

0022-3115/$ - see front matter © 2006 Elsevier B.V. All rights reserved.
doi:10.1016/j.jnucmat.2006.05.036

ation, liquid Pb–Bi eutectic (LBE) corrosion and embrittlement and non-negligible thermo-mechanical loads. The degradation of the mechanical properties of the T91 steel in the proton beam entrance area (beam window) has been considered as one of target lifetime limiting factors [3,4].

Compared to the T91 steel in the beam window, the SS 316L in the tubes will receive substantially less radiation damage although the LBE interaction effects and thermo-mechanical loads can be similar. The components made of SS 316L are considered as less critical [2]. As for the $AlMg_3$ alloy of the safety-container, both the existing experience from the operation of SINQ solid targets and preliminary studies on the radiation and water corrosion effects [5,6] indicate that this material should be reliable under the normal operating conditions of the MEGAPIE target.

For the safety and reliability studies of the MEGAPIE target, it is necessary to assess the lifetime of the LLMC beam window [3,4]. For this assessment it is difficult to adopt the usual design rules such as the ASME code Section 3 (for Nuclear Power Plant components, Division I, Boiler and Vessel code, 1986) because of the thin wall structure of the LLMC beam window. Therefore, it is necessary to use other approaches that will be discussed in detail in this paper.

2. Operating conditions of the LLMC beam window

2.1. Radiation damage and He production

The irradiation dose and He production in the structural materials of the MEGAPIE target has been calculated with different codes such as the FLUKA code [7] and the MCNPX code [8]. The calculations have been performed using a practical proton beam profile as shown in Fig. 1, which was deduced from measurements [9]. It can be seen from Fig. 1 that the peak current density is about 21 μA/cm^2 at 1 mA beam current delivered from the accelerator. Currently the accelerator delivers about 1.8 mA. Therefore, the peak current density at the SINQ target is about 37 μA/cm^2. Due to a 4 cm thick graphite target (Target-E) located in the beam line between the accelerator and the SINQ target, the proton beam current of accelerator is reduced by 30% when it is transported to the SINQ target. Meanwhile, the energy of protons decreases from 590 MeV to about 570 MeV.

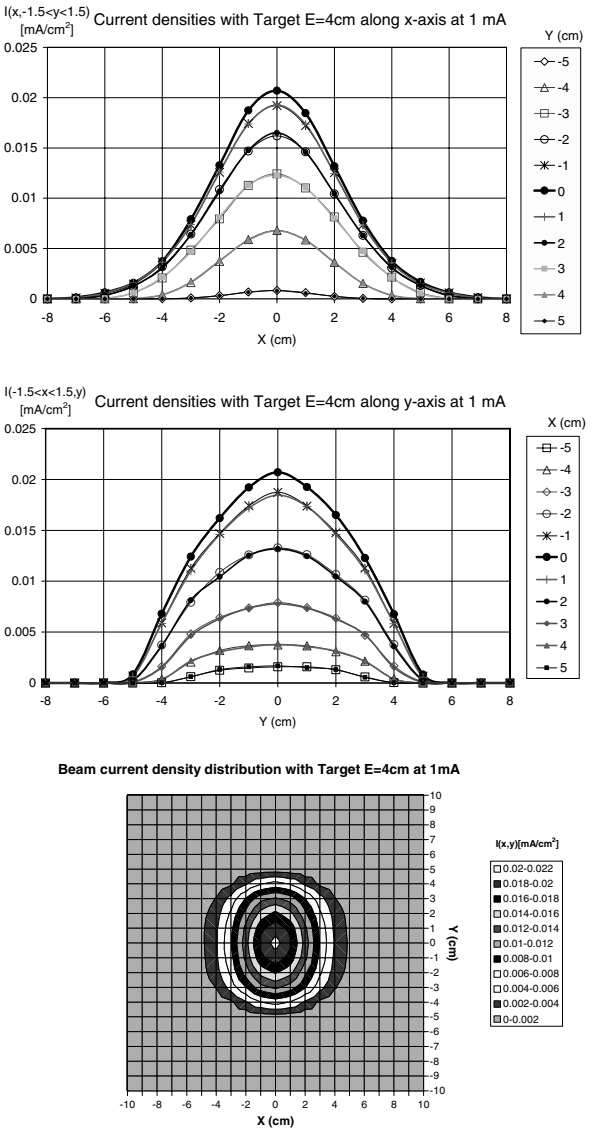

Fig. 1. The proton beam density profile at the SINQ target at 1 mA beam current delivered from the accelerator [9]. Upper: the beam density distribution along X-axis. Middle: the beam density distribution along Y-axis. Lower: the projection of the beam size and density on X–Y plan.

Fig. 2 shows the distributions of the radiation damage and helium production along the short beam axis at the beam window of the LLMC and the $AlMg_3$ safety-container after the target receiving 6 Ah proton charge, which was calculated with the FLUKA code. For the T91 beam window, the maximum dose of 15.6 dpa is slightly higher while the maximum He concentration of 1300 appm is lower than those calculated with the MCNPX code, 14.5 dpa and 1560 appm, respectively. It has been

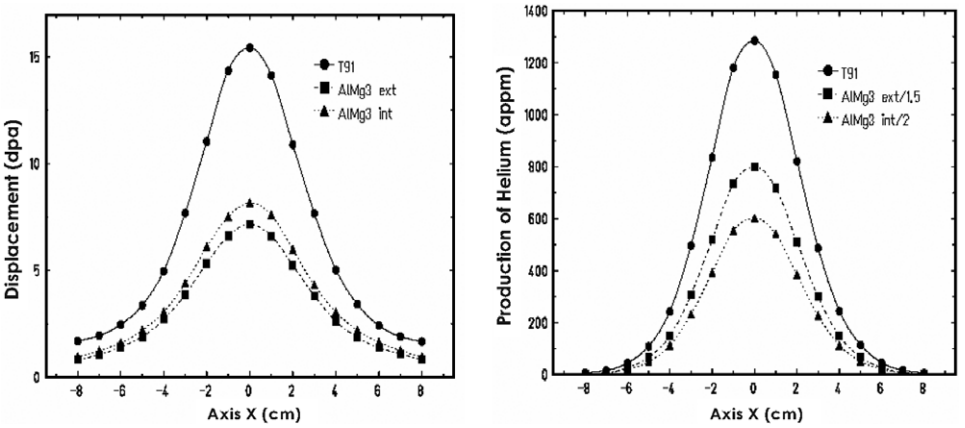

Fig. 2. Radiation damage and helium production distributions along the X-axis at the beam window of the T91 container and the $AlMg_3$ safety-hull after receiving 6 Ah proton charge. Calculation was done using the FLUKA code [7].

noted that the peak He concentration calculated with the updated production cross-sections measured from STIP samples is about 1600 appm.

2.2. Temperature distribution at the normal operating conditions

The temperature distribution at the beam window of the T91 container depends on several parameters such as the temperature of the inlet LBE flow, the proton beam intensity profile, the total beam current, and the main and by-pass LBE flow. The calculation has been performed with the CFX-4.4 code in conditions of: 235 °C annulus inlet and 247 °C by-pass inlet temperatures, 37.5 kg/s main flow rate and 2.5 kg/s by-pass flow rate [10]. Fig. 3 shows the temperature distributions of the outer surface (left) and the inner surface (right) of the beam window. At a proton beam current of 1.4 mA, (because of the 30% reduction from the graphite target), the maximum temperature in the beam window is about 375 °C at the outer surface and about 354 °C at the inner surface. Therefore the temperature gradient through the wall is about 21 °C. The by-pass flow brings the position of the peak temperature about 1.3 cm away from the beam center or the geometry centre of the window, as shown in Fig. 3.

2.3. Mechanical load at the beam window of the T91 container

The thermal mechanical load distribution in the beam window area has been calculated with the

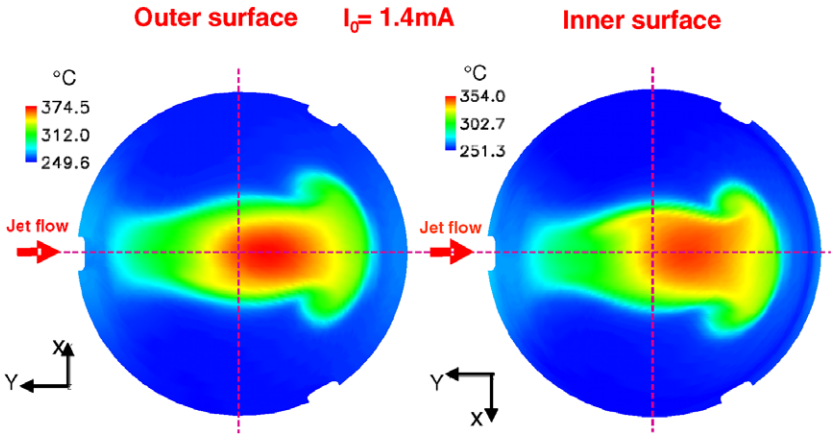

Fig. 3. Temperature distributions of the outer surface (left) and inner surface (right) of the beam window in the case of the by-pass flow parallel to the major axis of the beam [10].

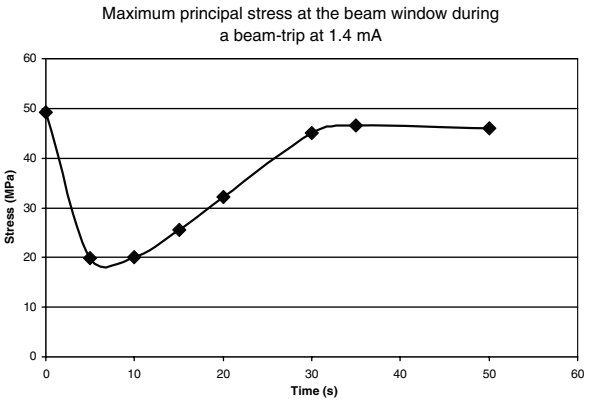

Fig. 4. The variation of the maximum principal stress at the beam window in the first minute after shut off the beam.

ABAQUS code [11]. The calculation indicates that the maximum Von Mises stress is generally below 50 MPa. In a 'beam-trip' transient case, the stress drops firstly to about 20 MPa, and then returns to almost the same initial stress level when the temperature is raised up to operating level by the central heating rod. Fig. 4 shows the stress variation in the first minute after the beam shut off.

3. Irradiation effects in relevant conditions

The temperature at the beam window will range from the temperature of the inlet LBE flow, 230 °C to the maximum 375 °C as shown in Fig. 3. In this temperature range, the main effect induced by the proton and neutron irradiation in the T91 steel will be hardening and embrittlement, which is the typical behavior of ferritic/martensitic (FM) steels irradiated in low temperature regime ($\leqslant 0.35\ T_m$, T_m is the absolute melting point temperature) [12]. In this section, the data of the T91 steel and some other FM steels obtained from the SINQ Target Irradiation Program (STIP) [13] in the relevant irradiation or test temperature range will be presented.

3.1. Tensile properties

Tensile tests are commonly used for determining the status of materials after irradiation. Fig. 5 presents the tensile test curves of the T91 steel irradiated in STIP-I up to 9.8 dpa/815 appm He at temperatures up to about 300 °C and tested at 22, 250 and 350 °C [14]. One can see that the yield stress increases with irradiation dose. Meanwhile, the uniform elongation drops to less than 1% even in the cases where the testing temperatures are slightly higher than the irradiation temperatures. Recently some HT-9 and EP 823 specimens irradiated in STIP-II to 19 dpa at 340 ± 45 °C were tested by Maloy et al. [15] at 25, 250 and 400 °C. The results reduction of uniform elongation to less than 1% when tested at 250 °C and 25 °C but some retention of ductility when tested at 400 °C. Furthermore, fission-neutron and ion irradiations normally demonstrate the same kind of results, for example the T91 steels irradiated in the HFIR in the USA [16] and with α-particles in Forschungszentrum Jülich, Germany [17].

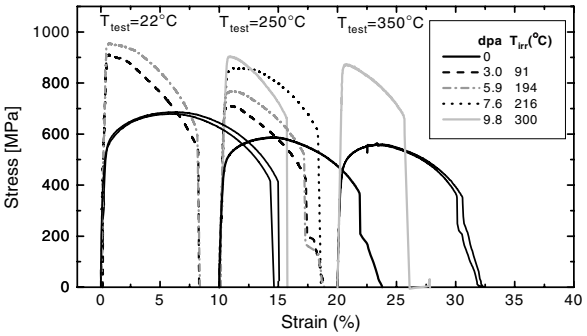

Fig. 5. Engineering tensile stress–strain curves of T91 specimens irradiated in SINQ Target-3 and tested at 22, 250 and 350 °C [14].

The tensile results indicate that the T91 steel still has considerable ductility at about 9 dpa in terms of total elongation of $\geqslant 6\%$, although the irradiation induced significant hardening and embrittlement. It has to be noted as well that the tensile curves were obtained from small specimens which generally give smaller total elongation values as compared to specimens with sizes defined in the ASTM standards.

3.2. Shift of the ductile-to-brittle transition temperature

One of the main concerns as regards the safe operation of the target is the risk of sudden brittle failure of the window. Therefore, it is necessary to evaluate the change of the ductile-to-brittle transition temperature (DBTT) of the T91 steel during irradiation. This can be assessed by impact Charpy tests, which is the standard method to determine DBTT of FM steels.

Fig. 6 presents the curves of absorbed energy as a function of testing temperature for T91 steel samples in conditions of unirradiated and irradiated to 4.6 and 6.8 dpa [18]. The figure demonstrates that the

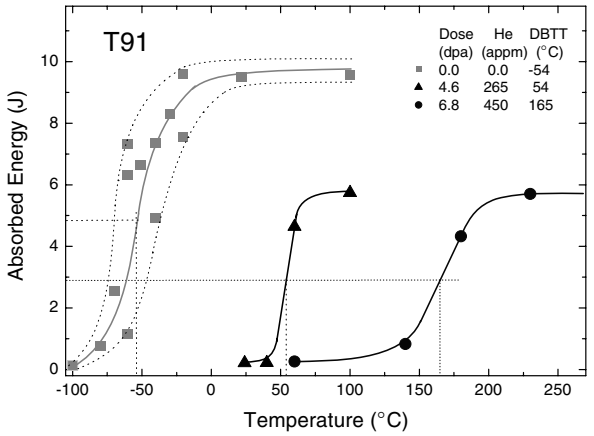

Fig. 6. Testing temperature dependence of the absorbed energy of the T91 Charpy samples at different irradiation doses in STIP-I [18].

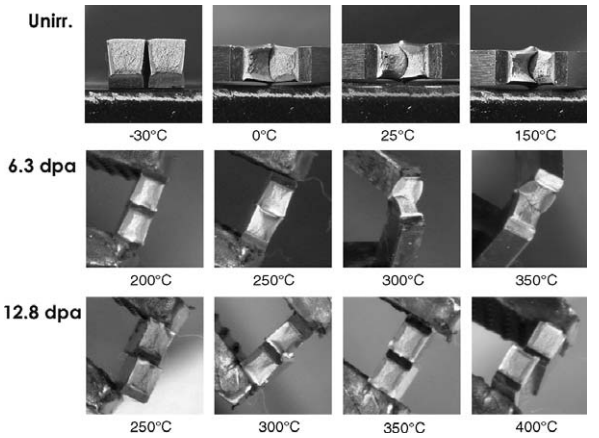

Fig. 8. Photographs show the fracture surfaces of the specimens after testing at different temperatures.

DBTT of the T91 steel in as-received condition is about −54 °C. After irradiation to 4.6 and 6.8 dpa, the DBTT increases to 54 and 165 °C, respectively. Meanwhile the upper shelf energy (USE) decreases after irradiation. However, the DBTT and the USE of a FM steel depends strongly on its chemical composition, manufacturing processing and heat treatments. In another case, the T91 steel was 30% cold worked after the standard heat treatment and then re-tempered. The notch of the specimens was in the T–L orientation. The specimens were irradiated in STIP-II to 6.3 dpa/300 appm He at ~118 °C and 12.8 dpa/785 appm He at ~210 °C. As shown in Fig. 7, the DBTT in the unirradiated condition is about −20 °C and the USE is about 6 J. After irradiation, the DBTT increases tremendously. The specimens of 6.3 dpa/300 appm He fractured in a brittle manner at ⩽250 °C, while the others of 12.8 dpa/785 appm He fractured in a brittle manner at all four temperatures between 250 and 400 °C, as can be seen from the photos in Fig. 8.

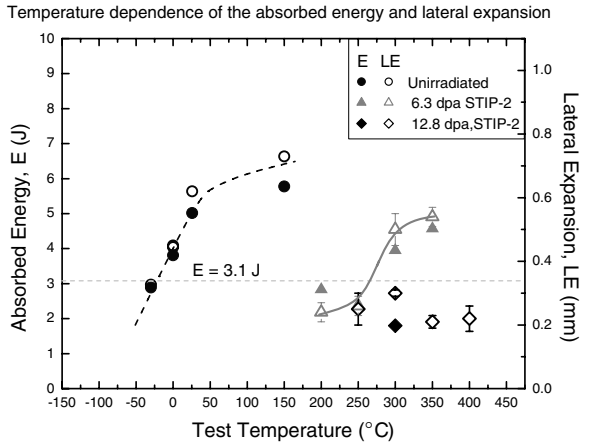

Fig. 7. Testing temperature dependence of the absorbed energy and lateral expansion of T91 Charpy impact specimens (in T–L orientation) irradiated in STIP-II.

Fig. 9 presents all the data of ΔDBTT (shift of DBTT) after irradiation obtained from both Charpy and SP tests on different FM steels irradiated in STIP-I and STIP-II. These plots compile data for different F/M steels generally in the standard heat treatment, but it should be noted that the initial heat treatment can strongly affect the ΔDBTT. T91 in the standard heat treatment exhibits a ΔDBTT of 300 °C at 9.5 dpa and 800 appm He but when the material is 30% cold worked and re-tempered a ΔDBTT of 300 °C is observed after only 6.5 dpa and 360 appm He.

3.3. Fracture toughness

The fracture toughness of materials reflects its resistance to crack extension. It is known that the fracture toughness of FM steels decreases after neutron irradiation [12] and even faster under high energy proton irradiation [19]. The change in the fracture toughness of the T91 steel and another two 8-9Cr steels (F82H and Optimax) irradiated in STIP-I up to 9.3 dpa/530 appm He at temperatures up to 250 °C has been evaluated [20]. Except one tested at room temperature, the other T91 specimens were tested at 250 °C because it is in the temperature range of the MEGAPIE beam window. The F82H and Optimax specimens were tested at

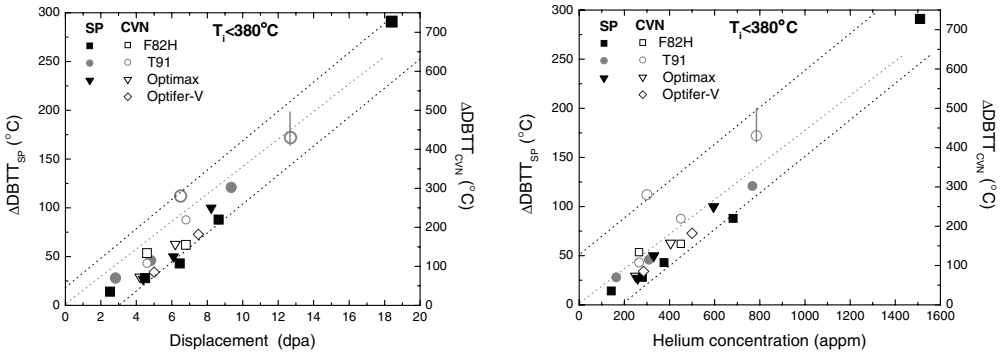

Fig. 9. Irradiation dose (left) and helium concentration (right) dependences of ΔDBTT obtained from Charpy impact and SP tests.

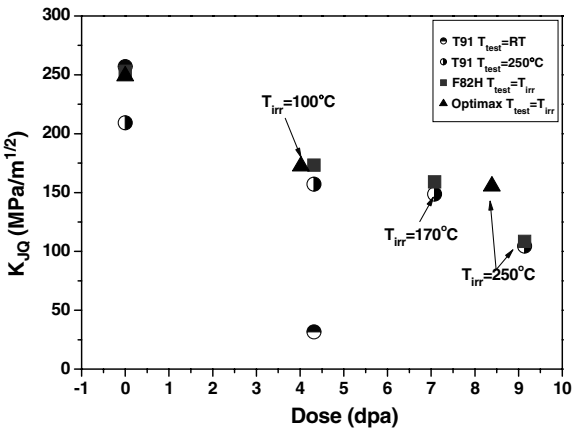

Fig. 10. The irradiation dose dependence of the fracture toughness the T91, F82H and Optimax steels after irradiation in STIP-I [20].

the irradiation temperatures between 100 and 250 °C.

Fig. 10 shows the measured fracture toughness data of the three steels before and after irradiation. In the present irradiation temperature range (100–250 °C) the fracture toughness of the martensitic steels decreases with irradiation dose. At room temperature, after irradiation to 4.3 dpa at about 100 °C, a T91 specimen broke in the elastic deformation regime and gave a fracture toughness value of about 30 MPa$\sqrt{m}$, within the lower-shelf region. Except for this specimen, all other specimens presented fracture toughness values above 100 MPa$\sqrt{m}$.

4. LBE corrosion and embrittlement effects in relevant conditions

Recent experiments demonstrated that, in the normal operating conditions of the MEGAPIE target the T91 beam window will be slightly corroded by LBE but could be seriously affected by LBE embrittlement. So far, most of the results obtained are from tests performed in flowing or static LBE without irradiation. Only few tests have been performed on irradiated materials or in in-beam condition.

4.1. LBE corrosion effects

In addition to such parameters as temperature, liquid metal flow rate and temperature gradient in the system, the oxygen concentration in LBE can also greatly affect the corrosion rate and corrosion mechanisms.

The mechanisms of LBE corrosion of FM steels can be divided into two oxygen regimes: (1) dissolution at low oxygen content in Pb–Bi ($<\sim10^{-8}$ wt%), and (2) oxidation at high oxygen content in Pb–Bi ($>\sim10^{-6}$ wt%). The oxygen saturation concentration at 300 °C is about $\sim10^{-6}$ wt%. The oxygen content in the MEGAPIE target should be such that it saturates at the LBE filling temperature, 250 °C. This oxygen concentration will be slowly reduced by the hydrogen production after irradiation starts resulting in a low oxygen content condition.

Corrosion tests performed in LBE are normally at $\geqslant$400 °C, because at these temperatures the corrosion rate of steels is high enough to allow relatively precise measurements, and meanwhile, the oxygen content in LBE can be monitored or measured by oxygen meters developed so far.

Few experiments have been carried out at 400 °C in LBE with low oxygen concentrations. In the LECOR loop, tests on T91 and SS 316L steels have been run up to 4500 h [21]. During the tests, the test section temperature was 400 °C and the temperature at the cold branch was 300 °C. Low oxygen concentration of 10^{-8}–10^{-10} wt% in LBE was achieved by

adding 80 wppm of magnesium. The flow velocity in the test sections was 1 m s^{-1}. The results of these tests show that both SS 316L austenitic stainless steel and T91martensitic steel exhibited weight losses after exposure in LBE. The value of weight loss after 1500 h and 4500 h for T91 were 0.027 mg/mm^2 and 0.184 mg/mm^2, while for SS 316L they where 0.022 mg/mm^2 and 0.155 mg/mm^2, as indicated in Fig. 11 [21]. The difference between the values after the two exposure times is believed to be due to the presence of a thin native oxide film on the surface of the specimens. The native oxide film can significantly protect from corrosion at the beginning period. Once the thin native oxide film is destroyed, linear corrosion kinetics may start and continue. From the figure one can see that the 'incubation' period is a few hundred hours in this experimental condition.

The corrosion rates calculated from the weight loss values between 1500 and 4500 h are 58 μm/yr for the T91 steel and 49 μm/yr for the SS 316L steel. Similar results were obtained from other tests in similar conditions [22].

Observations on the samples tested in the LECOR loop showed that a uniform attack and about 5 μm deep intergranular and transgranular penetrations were detected on their surfaces, as illustrated in Fig. 12.

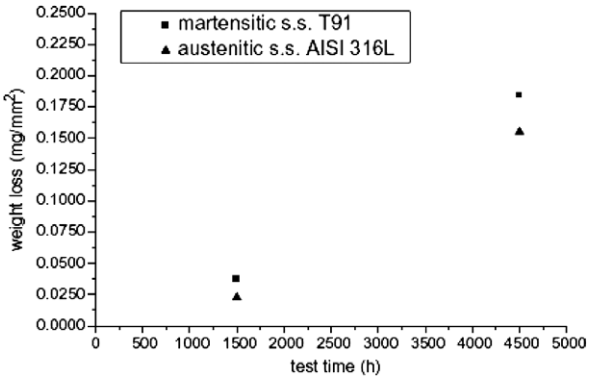

Fig. 11. Specific weight change of steels after exposure in the LECOR loop [21].

In LBE with a high oxygen content, oxide layers will form on the surfaces of steels, which will efficiently protect the steels against the mass transfer and intergranular attack induced by corrosion.

In the LiSoR (liquid–solid reaction under irradiation) experiments, T91 specimens were irradiated with 72 MeV protons in a LBE loop [24]. The temperature of the LBE was controlled at 300 °C and the oxygen concentration was saturated at this temperature. During irradiation the temperature in the irradiated areas of the specimens increased, which depended on the proton beam parameters and varied between 325 and 400 °C in the three experiments LiSoR-3 to LiSoR-5. Fig. 13 presents the micrographs showing the oxide layers formed on the surfaces of specimens of LiSoR-3 and LiSoR-5 after irradiation for 264 and 724 h at 325 and 380 °C, respectively. The oxide layer of the LiSoR-3 specimen is about 350 nm thick and that of the LiSoR-5 specimen is about 800 nm. This indicates that the oxide layer increases with irradiation temperature and time in LiSoR experiments.

4.2. LBE embrittlement effects

The LBE embrittlement effects of FM steels have been intensively studied recently. Mechanical tests such as tensile, bending and fatigue tests have been conducted on irradiated and unirradiated specimens in LBE in a temperature range from 200 to 450 °C.

4.3. Tensile tests in LBE

Tensile tests have been performed on specimens with different geometries, surface conditions and irradiation environments. Cylinder specimen of 3 mm in diameter after exposure in the LECOR

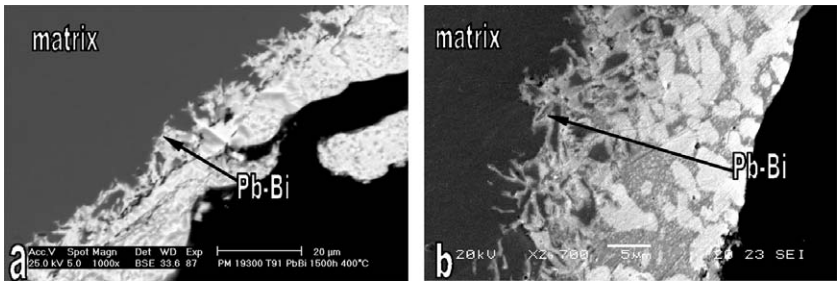

Fig. 12. SEM micrographs showing the surfaces of T91 specimens after exposure in LBE for 1500 and 4500 h in the LECOR loop [23].

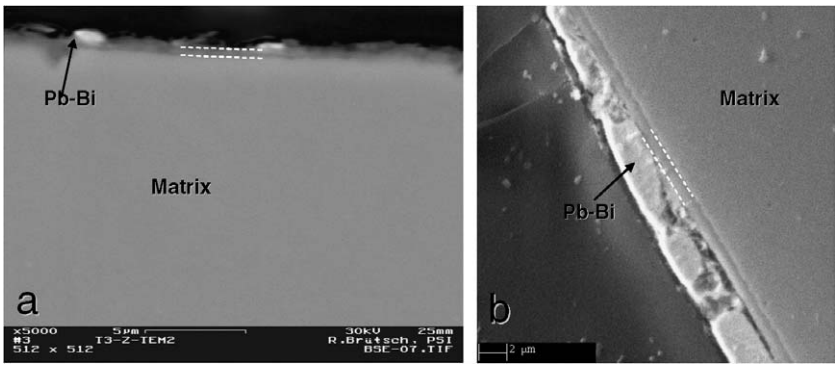

Fig. 13. Micrographs showing the cross-sections in the irradiation areas of (a) LiSoR-3 and (b) LiSoR-5 specimens.

loop for 1500 and 4500 h under low oxygen content were tested in Ar gas atmosphere at 400 °C. The tensile stress–strain curves presented in Fig. 14 indicate that the ductility in terms of total elongation decreases with the exposure time in LBE. This shows the LBE embrittlement effects even when the specimens were tested in Ar gas with a remaining film of LBE.

LBE embrittlement on the T91 steel was systematically observed at temperatures between 300 and 425 °C through slow strain rate (10^{-5}/s) tensile tests on flat type specimens with microcracks (induced by EDM cutting) on the lateral surfaces of the specimens. Fig. 15(a) and (b) illustrate the tests at 300 and 375 °C. But such embrittlement effect was not observed from the specimens without microcracks tested in the same conditions (Fig. 15(c) and (d)) [25]. The oxygen content in the LBE was about 10^{-6} wt%.

Similarly, slow strain rate tensile tests conducted on smooth cylinder T91 specimens in as-received and irradiated to 1.7 dpa conditions at 200 °C did not indicate any LBE embrittlement effects [26]. It is clear that surface flaws such as corrosion induced grain boundary attacks (Fig. 12) or microcracks on surfaces are important for the occurrence of LBE embrittlement.

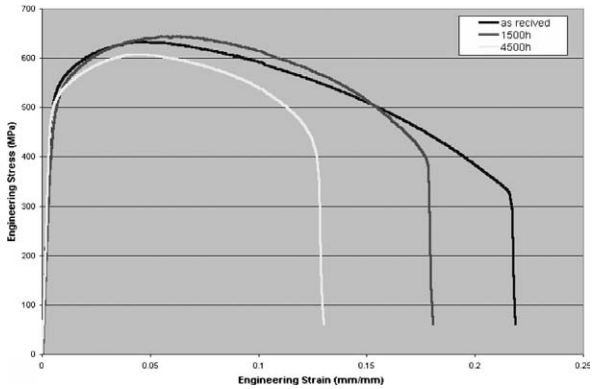

Fig. 14. Tensile curves of T91 specimens after exposure in LBE for 1500 and 4500 h in the LECOR loop and tested in Ar at 400 °C [23].

4.4. Fatigue tests in LBE

Most components in the MEGAPIE target will experience fatigue induced by instabilities in the proton beam (beam trips), although the stress level may not be high. Hence, it is necessary to understand the LBE effect on the fatigue lifetime of steels, especially the T91 steel, in the relevant temperature range.

A lot of fatigue tests have been carried out by a French group in Lille, France [27]. The fatigue specimens were smooth and cylindrical with a gauge length of 13 mm and a gauge diameter of 10 mm. The fatigue tests were performed at 300 °C in both air and LBE. The testing mode was push–pull with $Re = -1$ and the strain ranges varied from 0.4% to 2.5%. To study the possible LBE corrosion – plasticity interactions effect, one batch of specimens was pre-exposed in a LBE loop at 600 °C for 613 h at an oxygen concentration less than 10^{-10} wt%. And another batch of specimens was exposed in saturated oxygen LBE at 470 °C for 502 h. Therefore, the specimens in the first batch had corrosion pits on the surfaces while the ones in the second batch had oxide layers. Some tests were performed with a holding time of 10 min at the strain amplitude. The main observations are as the following:

(1) In general, the fatigue lifetime is reduced by a factor of two or more when testing in LBE as compared to that in air (Fig. 16(a)).

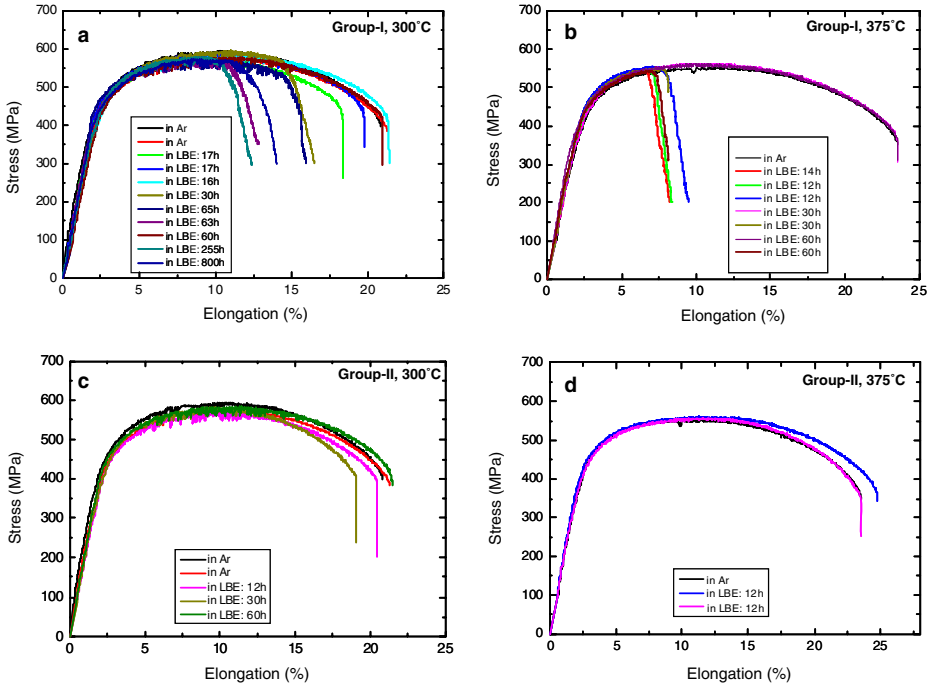

Fig. 15. Tensile stress–strain curves of T91 specimens with micro-surface-cracks (a) and (b) and without micro-surface-cracks (c) and (d) at 300 and 375 °C.

(2) In LBE, a reduction in fatigue lifetime is observed in the tests with hold time, although there is no difference in the tests done in air.
(3) Dissolution corrosion shows a strong effect on the reduction of the fatigue lifetime, while the oxide formation demonstrates clearly an effect in annihilating the detrimental effect of LBE on fatigue lifetime (Fig. 16(b)).
(4) There is a trend that the LBE effect becomes less significant at smaller strain amplitudes with continuous cycling (Fig. 16(a)).

In the LiSoR experiments, due to the small proton beam spot wobbled at a low frequency (1.2 or 2.5 Hz), the temperature and stresses in the irradiated areas of both the test section tube and the inner tensile-stressed specimen change in a very complex way [28]. Fig. 17 presents the variation of the temperature-increase and stresses in the irradiation area of the inner specimen of LiSoR-5, where the proton beam wobbled at 2.5 Hz. Both the temperature-increase and stresses oscillates with the wobbling proton beam. As the small irradiation area of about

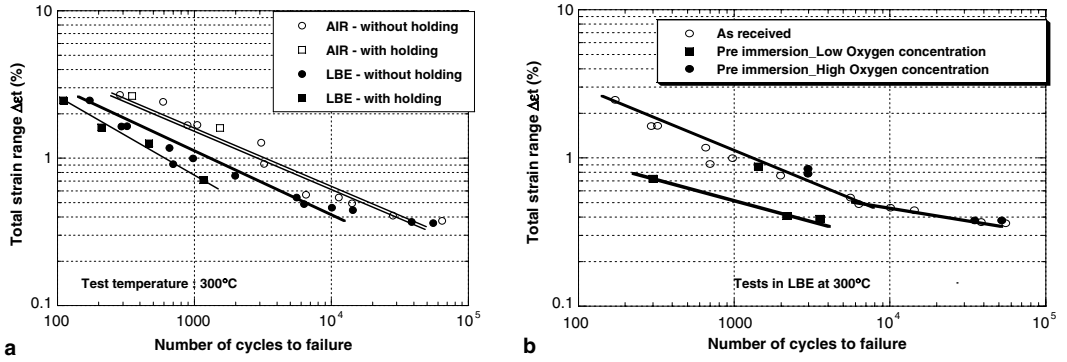

Fig. 16. (a) The fatigue life defined as the number of cycles from which a 25% drop in the quasi stabilized tensile stress occurs. (b) Effect of pre immersion in LBE at low and high oxygen concentrations on the fatigue lifetime in LBE at 300 °C of theT91 steel [27].

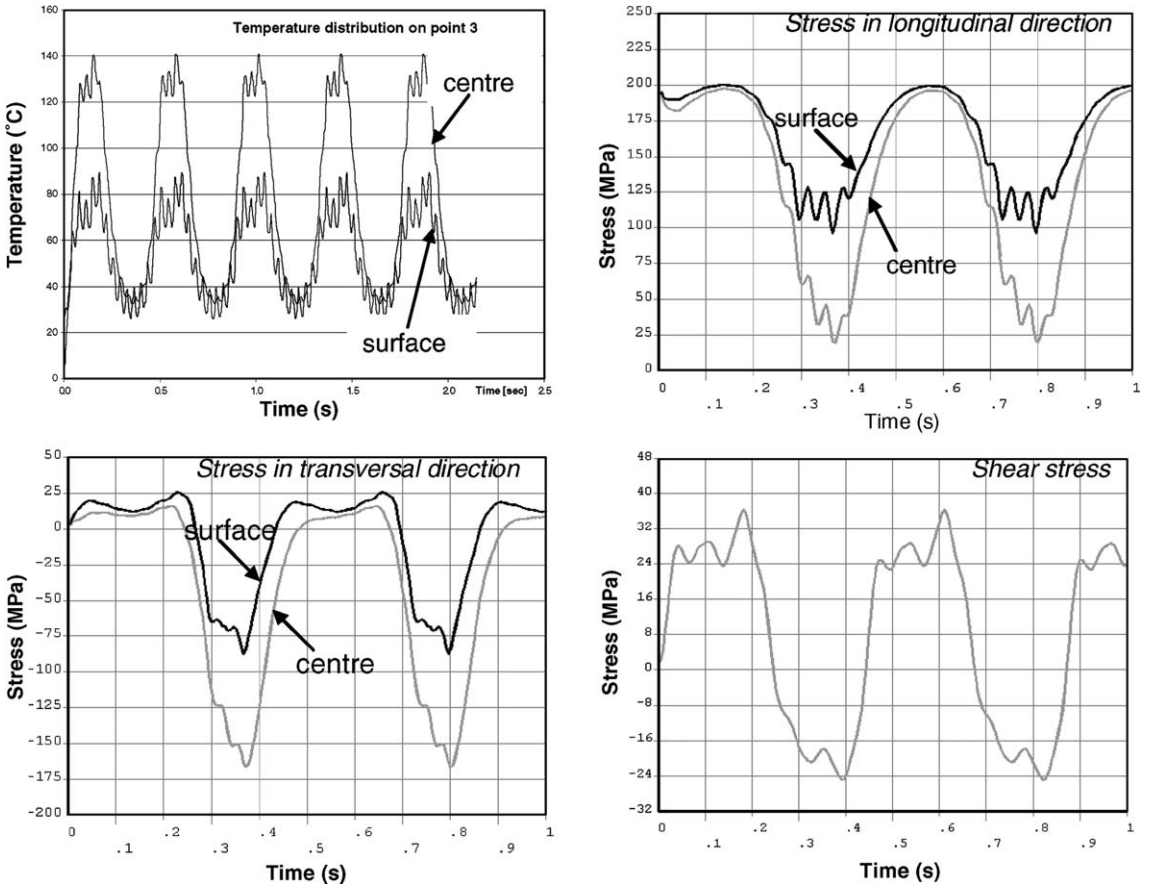

Fig. 17. The time dependence of temperature-increase, stresses in longitudinal/transversal directions and shear stress at a point in the irradiation area of the TS-specimen LiSoR-5 calculated with the ANSYS code [28].

$5.5 \times 14\ mm^2$ size located at the centre of the specimen of $20 \times 140\ mm^2$, the temperature-increase induces considerable compression stresses. Consequently, the 200 MPa tension stress applied mechanically in longitude direction of the specimen is reduced, on the other hand, in the transversal direction the compression stress is produced. Meanwhile, a shear stress is induced at a smaller magnitude and there is also a stress about 70 MPa cross the thickness of the half of the specimen. Since these stresses are localized and below the yield stress of the T91 steel at such temperatures, no evident deformation is expected. No microcrack was observed on the surface can be attributed to this reason.

The situations in LiSoR-3 and LiSoR-4 are less serious due to shorter irradiation time and less beam current as well.

In LiSoR-2 the situation was different due to using a smaller beam size and slower wobbling. The peak current density in the small beam spot was about 3.5 times as great as that of LiSoR-5. The temperature-increase and the stresses were much higher, which resulted in a crack induced in the irradiation area of the tube. The microstructure in both irradiation areas of the tube and the inner specimen demonstrated well developed dislocation cells which indicated heavy deformation [29]. However, no microcracks were observed in the irradiation area of the inner specimen where the maximum temperature calculated was 600-700 °C and the stress varied from 200 MPa to about 500 MPa. The reason for the crack generated in the tube can be attributed to, on one side, the high temperature and high stress, and on the other side, the pre-existed microcracks on the inner surface of the tube, which were produced by EDM cutting.

4.5. Bending tests

Only few bending tests were performed in LBE presently. The French group in Lille conducted 4-point bending fatigue tests on T91 specimen in

LBE at 300 °C [27]. The results show that crack growth rate is much higher for the tests in LBE, as can be seen from Fig. 18.

In another case, 3-point bending tests were performed on T91 specimens irradiated to 7.1 and 9.1 dpa in LBE at 250 °C. The oxygen concentration in the LBE was saturated. Fig. 19 presents the load–displacement curves of the specimens tested in both Ar [20] and LBE. As illustrated in the figure, LBE embrittlement effect is clear, particularly in the case of the 9.1 dpa specimen. For this specimen, the crack propagated suddenly through the whole specimen after three loading–unloading cycles, and resulted in a brittle fracture. The breaking procedure is believed to be such that after three loading–unloading cycles, the crack was slightly opened so that the LBE could enter the crack and wet the crack tip. Once the sharp crack tip was wetted, the crack could propagate at a high speed. To evaluate the fracture toughness, one may treat this as a brittle case by taking only the fast crack propagation part into account, because during the first three loading–unloading cycles the LBE might not yet effectively affected. In this case, the corresponding fracture toughness value is about 42 MPa$\sqrt{m}$, which is significantly lower than that of test in Ar, 105 MPa$\sqrt{m}$.

For the other specimen of 7.1 dpa, LBE also resulted in a quicker breaking as compared to the case in Ar. However, the LBE effects took place after about 12 loading–unloading cycles. At this dose the DBTT of the T91 steel is around 200 °C. Therefore the steel should be still ductile at 250 °C. So the crack tip might be relatively easier blunted, and consequently the LBE effect is less pronounced.

In Fig. 19, the maximum loads of the specimen depend on the irradiation dose and the pre-crack length. For the specimen of the same irradiation dose, it depends on the pre-crack length only. As the pre-crack length is slightly different for different specimen, it results in different maximum loads for different specimens.

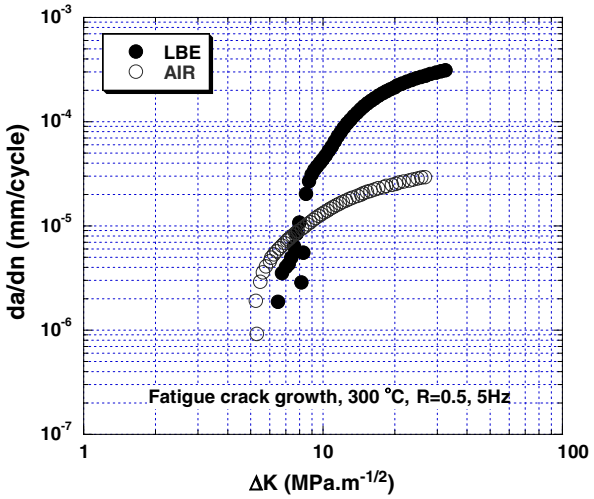

Fig. 18. Fatigue crack growth curves of the T91 at 300 °C in air and LBE ($f = 5$ Hz, $R = P_{min}/P_{max} = 0.5$) [27].

5. Discussion

The results presented in Sections 3 and 4 indicate clearly that each of following three effects: LBE corrosion, embrittlement and proton/neutron irradiation, can introduce significant, even life-limiting damage to the T91 beam window if certain requirements are fulfilled.

For LBE corrosion effects, the low oxygen concentration situation is of significant concern. The essential issues are two: reduction in thickness and

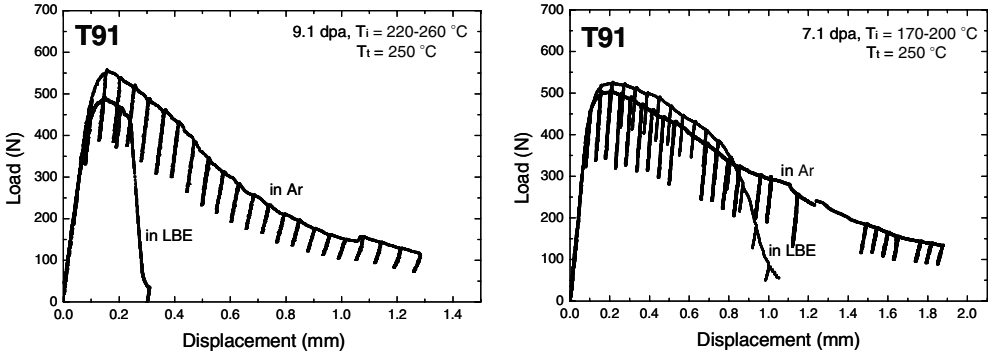

Fig. 19. Load–displacement curves of irradiated T91 specimens tested at 250 °C in Ar and LBE (oxygen saturate).

grain boundary selective dissolution. The corrosion rate measured at 400 °C under low oxygen concentration and about 1 m/s LBE flow velocity is less than 100 μm/yr. It was also found that the corrosion rate is proportional to $u^{0.87}D^{0.7}$, where u is the LBE velocity (m/s), and D the diffusion coefficient (m^2/s) of iron in LBE, which is proportional to temperature [22]. In the MEGAPIE case, the maximum LBE velocity at the inner surface will be about 0.6 m/s [10], while the temperature will be lower. Therefore, the iron diffusion coefficient in MEGAPIE case will be smaller. Therefore, it is believed that the maximum corrosion rate at the T91 beam window will not be higher than that in the LECOR loop, ~60 μm/yr. For 6-month planned operation it will be about 30 μm or less. This means that the wall thickness (1.5 mm) may be reduced about 2%. In fact, due to the initial oxygen content in the LBE, the irradiation area of the beam window will be oxidized in the beginning period which will delay the dissolution process. Thus the actual thickness reduction should be even smaller. The strength of the T91 beam window will not be a safety issue if the wall thickness is reduced by 2%.

Comparing to the thickness reduction, the grain boundary penetration could be more dangerous because it initiates microcracks on the surface, which can promote LBE embrittlement. LBE can induce brittle fracture in the T91 steel, particularly in the irradiated condition. But the brittle fracture may only take place when a critical stress level is reached. At a low stress level (50 MPa), in the thin beam window of MEGAPIE a brittle fracture is unlikely to occur within a short irradiation period. This has been demonstrated by a linear elastic fracture mechanics (LEFM) analysis [4].

In the LEFM analysis, the presence of a crack at the surface of the window was assumed and the stress intensity factor was calculated for mechanical loads corresponding to normal operating conditions. The stress intensity factor values as a function of crack depth are plotted in Fig. 20. The results imply that the fracture toughness of the T91 steel of the beam window can be allowed to reduce to less than 10 MPa$\sqrt{m}$ when a surface crack is as deep as half of the wall thickness (1.5 mm). From Sections 3 and 4 we know that the fracture toughness of the T91 steel will maintain at a level much higher than 10 MPa$\sqrt{m}$ at 9 dpa.

It is not so clear whether the LEFM analysis can be taken as a guideline for the lifetime assessment. It is difficult to imagine that the fracture toughness of T91 steel could drop to few MPa$\sqrt{m}$. The lower-shelf fracture toughness value of T91 and other FM steels are normally about 40 MPa$\sqrt{m}$ [12]. So far it seems no such fracture toughness values below 20 MPa$\sqrt{m}$ were obtained from 7-12Cr FM steels in either unirradiated or irradiated conditions. Of course, the fracture behavior of a component depends strongly on its geometry. Generally thinner structures can allow for lower fracture toughness.

Nevertheless, for a safe operation of the MEGAPIE target it is strongly recommended that the T91 steel in the beam window should work in a *ductile* condition rather than in a *brittle* one. This means either the DBTT should not reach the operation temperature or the fracture toughness should not drop below 40 MPa$\sqrt{m}$.

Using the DBTT judgment: Since the lowest operating temperature will be 230 °C in beam-off condition, and the DBTT of the unirradiated material is about −50 °C, a shift of 280 °C is required to raise

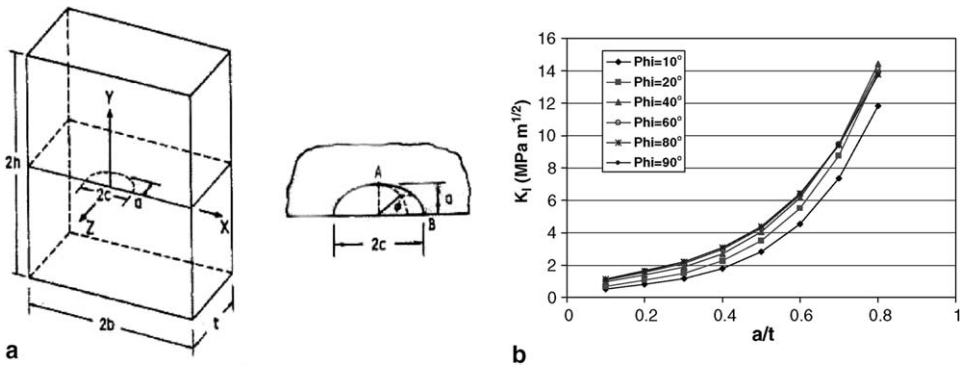

Fig. 20. (a) Semi-elliptical surface crack of depth a and length $2c$. (b) Stress intensity factor for a large ($c \gg a$) surface crack as a function of crack depth a in the window of thickness $t = 1.5$ mm [4].

the DBTT to 230 °C. Using the data of T91 specimens in the normal heat treatment condition, a dose of about 9 dpa is needed for a corresponding increase in DBTT. It corresponds to a proton charge of 3.5 Ah received by the target.

Using fracture toughness judgment: As the T91 specimen of 9.1 dpa tested in LBE gave a fracture toughness value of 42 MPa$\sqrt{m}$, this can be taken as the limit, which is basically the same as the other deduced from the DBTT data.

In above discussion no safety margin was taken into account. If one takes a 30% margin, it reduces the dose limit to about 6 dpa, corresponding to about 2.4 Ah. This can be considered as the lower bound of the lifetime of the T91 beam window.

There is not meaning to give an upper bound because: (1) the fracture toughness of the T91 steel at the beam window is not expected to degrade to the low value given by the LEFM analysis during the planned irradiation period, and (2) the $AlMg_3$ safety-container can save the SINQ facilities if the beam window has a leakage.

6. Conclusions

In this report, the lifetime of the beam window of the T91 liquid Pb–Bi container in the MEGAPIE target is discussed based on the present knowledge of LBE corrosion, embrittlement and radiation effects in the relevant condition. It is suggested that the lower bound of the lifetime of the T91 beam window is considered as when the steel becomes brittle at the lowest operation temperature, 230 °C, and with a safety margin of 30%. Evaluated from the DBTT data and fracture toughness values of T91 specimens tested in LBE, it gives a dose limit of about 6 dpa, corresponding to 2.4 Ah proton charge to be received by the target in about 20 weeks in the normal operation condition.

Acknowledgements

The authors would thank Dr Stuart Maloy for carefully reading the manuscript and useful discussion.

References

[1] G.S. Bauer, M. Salvatores, G. Heusener, J. Nucl. Mater. 296 (2001) 17.
[2] Synthesis report of working group X7 and X10 of the MEGAPIE project, submitted for publication.
[3] Y. Dai, Discussion on the lifetime of the target based on preliminary STIP results, FZKA 6876, Forschungszentrum Karlsruhe, 2003, p. 172.
[4] J. Henry, P. Lamagnere, Risk of brittle failure of the Pb–Bi container window: a tentative assessment, FZKA 6876, Forschungszentrum Karlsruhe, 2003, p. 184.
[5] Y. Dai, D. Hamaguchi, J. Nucl. Mater. 343 (2005) 184.
[6] Y. Dai, R. Restani, EPMA Inspection of the beam window of the $AlMg_3$ safety container of SINQ Target-4, PSI Technical Report, TM-34-05-09, 2005.
[7] Y. Foucher, Nuclear assessment of the MEGAPIE target, FZKA 6876, Forschungszentrum Karlsrihe, 2003, p. 149.
[8] E. Pitcher, MEGAPIE PIE meeting at PSI, 2003.
[9] U. Rohrer, private communication.
[10] T. Dury, private communication.
[11] A. Zucchini, private communication.
[12] R.L. Klueh, D.R. Harries, High-Chromium Ferritic and Martensitic Steels for Nuclear Applications, ASTM Stock Number: MONO3, Bridgeport, NJ, 2001.
[13] Y. Dai, G.S. Bauer, J. Nucl. Mater. 296 (2001) 43.
[14] Y. Dai, X. Jia, K. Farrell, J. Nucl. Mater. 318 (2003) 192.
[15] S.A. Maloy, T. Romero, M.R. James, Y. Dai, J. Nucl. Mater., these Proceedings, doi:10.1016/j.jnucmat.2006.05.003.
[16] K. Farrell, T.S. Byun, J. Nucl. Mater. 318 (2003) 274.
[17] P. Jung, J. Henry, J. Chen, J.-C. Brachet J. Nucl. Mater. 318 (2003) 241.
[18] Y. Dai, P. Marmy, J. Nucl. Mater. 343 (2005) 247.
[19] S.A. Maloy, M.R. James, G. Willcutt, W.F. Sommer, M. Sokolov, L.L. Snead, M.L. Hamilton, F. Garner, J. Nucl. Mater. 296 (2001) 119.
[20] X. Jia, Y. Dai, J. Nucl. Mater., these Proceedings, doi:10.1016/j.jnucmat.2006.05.002.
[21] A. Aiello, M. Azzati, G. Benamati, A. Gessi, B. Long, G. Scaddozzo, J. Nucl. Mater. 335 (2004) 169.
[22] T. Malkow, H. Steiner, H. Muscher, J. Konys, J. Nucl. Mater. 335 (2004) 199.
[23] B. Long, G. Scaddozzo, C. Faziol, M. Agostini, A. Aiello, G. Benamati, Corrosion behaviour of steels and refractory metals in flowing Pb–Bi, FZKA 6876, Forschungszentrum Karlsrihe, 2003, p. 199.
[24] H. Glasbrenner, Y. Dai, F. Groeschel, J. Nucl. Mater. 343 (2005) 267.
[25] Y. Dai, B. Long, F. Groeschel, J. Nucl. Mater., these Proceedings, doi:10.1016/j.jnucmat.2006.05.039.
[26] D. Sapundjiev, A. Almazouzi, S. Van Dyck, J. Nucl. Mater., these Proceedings, doi:10.1016/j.jnucmat.2006.05.030.
[27] J.B. Vogt, A. Verleene, I. Serre, F. Balbaud-Célérier, A. Terlain, Coupling effects between corrosion and fatigue in liquid Pb–Bi of T91 martensitic steel, in: Proc. Eurocorr2005, Lisbonne, September 2005.
[28] K. Samec, Temperature calculations of the LiSoR experiment, PSI Technical Report, TM-34-05-02, 2005.
[29] Y. Dai, H. Glasbrenner, V. Boutellier, R. Bruetsch, X. Jia, F. Groeschel, J. Nucl. Mater. 335 (2004) 232.